

## SPATIAL AND TEMPORAL RESOLUTION OF A FAST-RESPONSE AERODYNAMIC PRESSURE PROBE IN GRID-GENERATED TURBULENCE

Florian M. Heckmeier\*, Stefan Hayböck, Christian Breitsamter

Chair of Aerodynamics and Fluid Mechanics  
Department of Mechanical Engineering  
Technical University of Munich  
Boltzmannstr. 15, 85748 Garching, Germany  
\*florian.heckmeier@aer.mw.tum.de

**Keywords:** fast-response multi-hole pressure probe, grid turbulence, measurement resolution

### ABSTRACT

The spatial and temporal resolution of a fast-response aerodynamic pressure probe (FRAP) is investigated in a benchmark flow of grid-generated turbulence. A grid with a mesh size of  $M = 6.4 \text{ mm}$  is tested for two different free-stream velocities, hence, resulting in Reynolds numbers of  $Re_M = \{4300, 12800\}$ . A thorough analysis of the applicability of the underlying assumptions with regard to turbulence isotropy and homogeneity is carried out. Taylor's frozen turbulence hypothesis is assumed for the calculation of deducible flow quantities, like the turbulent kinetic energy or the dissipation rate. Furthermore, besides the examination of statistical quantities, velocity spectra of measurements downstream of the grid are quantified. Results of a small fast-response five-hole pressure probe equipped with piezo-resistive differential pressure sensors are compared to single-wire hot-wire constant temperature anemometry data for two different wire lengths. Estimates of temporal and spatial turbulent scales (e.g. Taylor micro scale and Kolmogorov length scale) show good agreement to data in the literature but are affected by filtering effects. Especially in the energy spectra, very high bandwidth content cannot be resolved by the FRAP, which is mainly due to bandwidth limits in the temporal calibration of the FRAP and the minimal resolution of the integrated sensors.

### NOMENCLATURE

$A$		Coefficient for TKE decay fit
$b$	[m]	Wind tunnel nozzle width
$DA$		Degree of anisotropy
$d$	[m]	Diameter of the grid wires
$d_w$	[m]	Hot-wire diameter
$E_{corr}$	[V]	Corrected hot-wire voltage
$E_{HW}$	[V]	Hot-wire voltage
$E_{kin}$	[m <sup>3</sup> /s <sup>2</sup> ]	Kinetic energy spectra
$f$	[Hz]	Frequency

$f_s$	[Hz]	Sampling frequency
$f_{lp}$	[Hz]	Low-pass frequency
$G$		Hot-wire signal conditioning gain
$h$	[m]	Wind tunnel nozzle height
$k$	[m <sup>-1</sup> ]	Wave number
$K$	[m <sup>2</sup> /s <sup>2</sup> ]	Turbulent kinetic energy
$l_w$	[m]	Hot-wire length
$M$	[m]	Mesh size
$n$		Exponent for TKE decay fit
$O$	[V]	Hot-wire signal conditioning offset voltage
$Re_M$		Reynolds number based on the mesh size $M$
$Re_\lambda$		Reynolds number based on the Taylor micro scale $\lambda$
$Tu$		Turbulence intensity
$t_s$	[s]	Sampling time
$T_W$	[K]	Hot-wire temperature
$T_{ref}$	[K]	Reference temperature
$T_{meas}$	[K]	Temperature at the measurement
$u_i$	[m/s]	Velocity component
$u'_i$	[m/s]	Velocity fluctuations
$\langle u_i'^2 \rangle$	[m <sup>2</sup> /s <sup>2</sup> ]	Velocity variance
$U$	[m/s]	Velocity magnitude
$x, y, z$	[m]	Cartesian coordinates
$x_0$	[m]	Virtual origin of turbulence decay
$\varepsilon$	[m <sup>2</sup> /s <sup>3</sup> ]	Dissipation rate
$\eta$	[m]	Kolmogorov length scale
$\lambda$	[m]	Taylor micro scale
$\nu$	[m <sup>2</sup> /s]	Kinematic viscosity
$\sigma$		Solidity of the weaved grid

### INTRODUCTION

The unsteady flow field in the wake of objects is of great interest in experimental aerodynamics. Therefore, measurement techniques that are capable of acquiring this unsteadiness can help to understand highly fluctuating phenomena. Beside optical techniques, e.g. particle image velocimetry,

intrusive measurement techniques have been developed in the past decades. The best known method is hot-wire constant temperature anemometry (CTA). In order to overcome the downsides of hot-wire probes (e.g. fragility and high calibration effort), fast-response multi-hole aerodynamic probes (FRAP) have been investigated in several research groups worldwide (see e.g. Johansen (2001) and Kupferschmied et al. (2000)). Compared to steady pressure probes, a temporal calibration of the acoustic behavior of the line-cavity system inside the probe is determined in addition to the spatial calibration (Heckmeier et al. (2019)). Due to resonance and damping effects in the acoustic system and due to the outer dimensions of the probe, both spatial and temporal filtering effects of the velocity fluctuations are expected. The measurement of turbulent flows with turbulence length and time scales (e.g. Kolmogorov length scale  $\eta$ ) smaller than the corresponding probe sensing length and bandwidth is challenging. In order to quantify hot-wire probe resolution, Ashok et al. (2012) and Bailey et al. (2010) examined various hot-wire CTA probes with different wire lengths in grid-generated turbulence. Hence, in this paper, a similar wind-tunnel set-up is used to characterize and validate the FRAP spatial and temporal measurement behavior. A comparison to hot-wire data and to data from the literature is conducted.

In the first part of this paper, general information on grid-generated turbulence is given. Thereafter, general information on the calibration, the specification and assembly of the FRAP and the used hot-wire probes are discussed. The experimental set-up in the wind tunnel of the Chair of Aerodynamics and Fluid Mechanics (TUM-AER) is described. In the last part, the results regarding spatial and temporal resolution of the probe are discussed and an outlook is given.

## GRID-GENERATED TURBULENCE

As mentioned, grid-generated turbulence is well documented in the literature. Therefore, a theoretical introduction is given, before discussing the experimental results. A statistical analysis of grid-generated turbulence can be performed by evaluating higher order moments (like second and third central statistical moment). The nomenclature for the velocity vector is  $(u_1, u_2, u_3)$ , and the velocity can be expressed by its mean value and the fluctuation around the mean  $u_i = \langle u_i \rangle + u_i'$ . The magnitude of the velocity vector is denoted as  $U$ .

The degree of anisotropy  $DA$  measures if isotropy is given and relates the variances of the velocity fluctuations  $\langle u_i'^2 \rangle$ :

$$DA = \frac{2\langle u_1'^2 \rangle}{\langle u_2'^2 \rangle + \langle u_3'^2 \rangle} \quad (1)$$

For an isotropic flow,  $DA$  approaches 1. For grid-generated turbulence, values  $DA > 1$  are stated in the literature (see Ting 2016).

As a measure for the homogeneity, the third central moment of the velocity fluctuation can be used. When both isotropy and homogeneity can be assumed, the turbulent kinetic energy  $K$  is approximated by the following equation:

$$K = \frac{\langle u_1'^2 \rangle + \langle u_2'^2 \rangle + \langle u_3'^2 \rangle}{2} \approx \frac{3}{2} \langle U'^2 \rangle \quad (2)$$

Furthermore, the decay of turbulent kinetic energy can be expressed as a function of the normalized distance downstream of the grid:

$$\frac{K}{\langle U \rangle^2} = A \left( \frac{x - x_0}{M} \right)^n \quad (3)$$

Here,  $x_0$  describes the virtual origin of the turbulent kinetic energy decay. The coefficients  $A$  and  $n$  can be fitted with measurement data, as can be seen in Figure 1. The coefficient  $A$  depends on the grid dimensions and the applied Reynolds number. According to the literature, the exponent lies between  $1.15 < n < 1.45$  (see Pope (2000)).

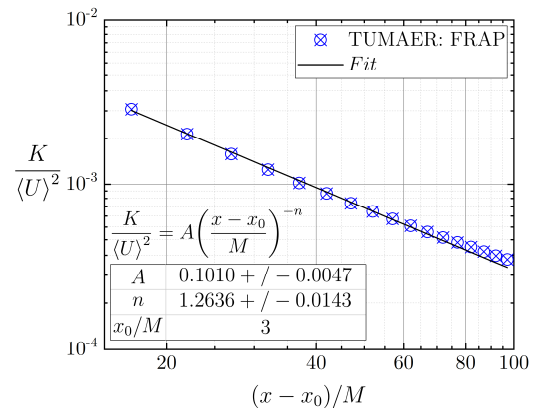


**Figure 1. Decay of the turbulent kinetic energy  $K$  as a function of the normalized streamwise distance  $(x - x_0)/M$**

By using Taylor's hypothesis of "frozen turbulence", the dissipation rate  $\varepsilon$  for homogeneous, isotropic turbulence can be calculated and the spatial development of the flow can be inferred from the temporal properties. Furthermore, the dissipation rate can be approximated by assuming a homogeneous isotropic turbulent (HIT) flow.

$$\varepsilon = -\langle U \rangle \frac{d}{dx_1} \frac{\langle u_1'^2 \rangle + \langle u_2'^2 \rangle + \langle u_3'^2 \rangle}{2} \approx -\langle U \rangle \frac{d}{dx_1} \frac{3}{2} \langle U'^2 \rangle \quad (4)$$

Hereby, turbulent length scales can be defined, which describe the size of eddies in the turbulent energy cascade. The Taylor micro scale  $\lambda$  indicates

the size of the largest vortex structures in the dissipative range and can be expressed as a function of the dissipation rate  $\varepsilon$  and the kinematic viscosity  $\nu$ :

$$\lambda = \sqrt{15\nu \frac{\langle u_1'^2 \rangle}{\varepsilon}} \quad (5)$$

Furthermore, a turbulence Reynolds number  $Re_\lambda$  that is calculated with the Taylor micro scale is given by:

$$Re_\lambda = \frac{\lambda \cdot \sqrt{\langle u_1'^2 \rangle}}{\nu} \quad (6)$$

As a measure for the lower size limit of the dissipation range, the Kolmogorov length scale  $\eta$  is defined. Here, the turbulent kinetic energy is dissipated into heat due to dominating viscous effects.

$$\eta = \left( \frac{\nu^3}{\varepsilon} \right)^{1/4} \quad (7)$$

For the spectral examination of the grid-generated turbulence, the normalized kinetic energy is calculated and shown as a function of the non-dimensional variable  $k\eta$ . Hereby, the wave number  $k$  is defined as  $k = 2 \cdot \pi \cdot f / \langle U \rangle$ . For de-noising the measured signals, the following procedure is applied on the signals: The velocity signal is split in evenly distributed parts and averaged in time space. Moreover, further filtering in the frequency space is applied. Figure 2 shows the filtering procedure exemplary for a measurement downstream of the grid. The grey “mean” curve is the initial averaged signal after transformation in frequency space. A median filter (red) and a Savitzky-Golay (blue) filter are further applied on the signal. In addition, the  $k^{-5/3}$  slope in the inertial range of the energy cascade is included.

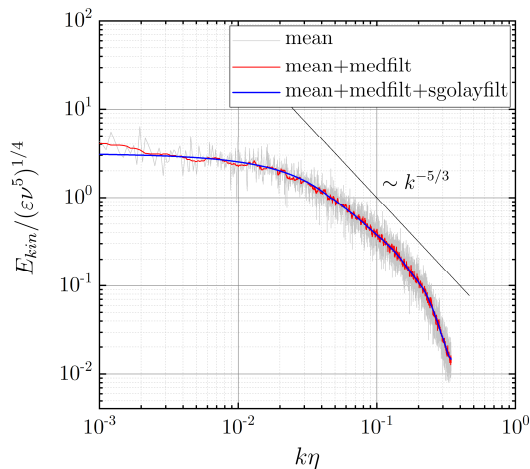


**Figure 2. Application of averaging and filtering for de-noising the non-dimensional kinetic energy spectra**

## EXPERIMENTAL SETUP

In the first part of this section, the measurement equipment for the grid-generated turbulence investigations is explained. The focus lies on the multi-hole pressure probe. Moreover, since the pressure probe data are compared to hot-wire CTA probe measurements, the basic characteristics of the used CTA equipment is given. In the second part, the wind tunnel setup with the grid is documented.

A fast-response five-hole probe, as depicted in Figure 3, is assembled to measure the flow field downstream of the grid. The probe head of the FRAP is additive manufactured. The hemispheric probe head and the cavities for the placement of the pressure sensors are post-manufactured in a cutting step. The probe is equipped with five piezo-resistive pressure sensors (Meggit Endevco 8507C-2), which are operated with the ambient pressure outside of the wind tunnel. They are connected to NI 9237 data acquisition cards, which transmit the data to the Labview controlled computer.

Table 1 shows the pressure probe properties. The probe is calibrated in a calibration wind tunnel for multiple velocity and angle combinations (Heckmeier et al. (2019)). Furthermore, a temporal calibration of the line-cavity system inside the probe is performed in a frequency test rig for frequencies up to 10 kHz in order to compensate resonance and attenuation effects.

**Table 1. Five-hole probe properties**

Tip diameter	3 mm
Channel diameter	≤ 1 mm
Sensor type	Piezo-resistive
Sensor pressure range	2 psig
Sensor diameter	2.3 mm
Spatial/angular calibration	±60°
Temporal calibration	10 kHz

For the reconstruction of the flow-field properties, the measured pressures are post-processed taking the calibration data of both, temporal and spatial, calibrations into account. A high reconstruction accuracy below 0.2° in both flow angles and 0.1 m/s in the reconstructed velocity can be achieved, as shown in Heckmeier and Breitsamter (2020). Pre-tests have shown that the probe is temporally limited due to bandwidth restrictions of the transfer function in the temporal calibration. Furthermore, the minimal resolution of the sensor and the DAQ-card must be taken into account, since the expected pressure fluctuations in the kHz-range could be lower than the minimal resolvable pressure fluctuation. For this case, an additional digital low pass filter is applied on the pressure data before reconstruction of the flow field properties. Hence, the temporal resolution restriction comes either from

the bandwidth of the temporal calibration or the minimal resolvable pressure fluctuation.

As a counterpart to pressure measurement systems, hot-wire probes are used to validate the FRAP results. A Dantec P11 single-wire probe with a standard wire length of  $1.2\text{ mm}$  and a retrofitted, shortened probe with a wire length  $0.7\text{ mm}$  are compared (see Table 2).

**Table 2. Single-wire probe properties P11**

Wire diameter		$5\ \mu\text{m}$
Wire length	shortened	$0.7\text{ mm}$
	standard	$1.2\text{ mm}$
Sensor temperature coefficient $\alpha_{20}$		$0.0036\ \frac{1}{\text{K}}$
Overheat ratio		1.8

The CTA hot-wire probe is operated with a Dantec StreamLine Pro constant temperature anemometer. The signal is digitized by a Data-Translation DT9836 16-bit A/D-converter. After bridge-balancing of the CTA-bridges, the probes are calibrated in the desired velocity range. Step-responses lie above the low-pass frequency. In order to compensate for temperature changes during the calibration and the wind tunnel measurements, the voltages are corrected as described in Bearman (1971):

$$E_{corr} = C \cdot E_{HW} - (1 - C) \cdot O \cdot G \quad (8)$$

where:  $C = \sqrt{\frac{T_w - T_{ref}}{T_w - T_{meas}}}$

The experiments on the grid-generated turbulence are conducted in the *Wind Tunnel B* of TUM-AER. The low-speed wind tunnel, which is of Göttingen type (closed-loop), has a cross section of  $h \cdot b = 1.20\text{ m} \cdot 1.55\text{ m}$ . Turbulence intensity without the grid lies below  $Tu = 1\%$ . At the nozzle section, a weaved grid with a mesh size  $M = 6.4\text{ mm}$  and a wire diameter of  $d = 1.6\text{ mm}$  is installed (see Figure 4). Hence, the solidity of the mesh is  $\sigma = \left(\frac{d}{M}\right) \left(2 - \frac{d}{M}\right) = 0.438$ . The free-stream velocity is monitored with a Prandtl probe that is installed upstream of the grid near the nozzle. The free-stream velocities are set to match the Reynolds numbers  $Re_M = \{4300, 12800\}$ . For all types of probes, measurements are acquired along an  $x$ -traverse downstream of the grid. The  $x$ -positions are normalized by the mesh size  $M$  and lie between  $x/M = (20, 100)$ . Both hot-wire and FRAP data are sampled with a sampling frequency of  $f_s = 50\text{ kHz}$ . In order to account for aliasing problems, a low-pass filter below the Nyquist frequency ( $f_{lp} \leq f_s/2$ ) is set for both acquisition setups. The measurement time was set to  $t_s = 15\text{ s}$ .



**Figure 3. Fast-response five-hole probe equipped with piezo-resistive sensors**

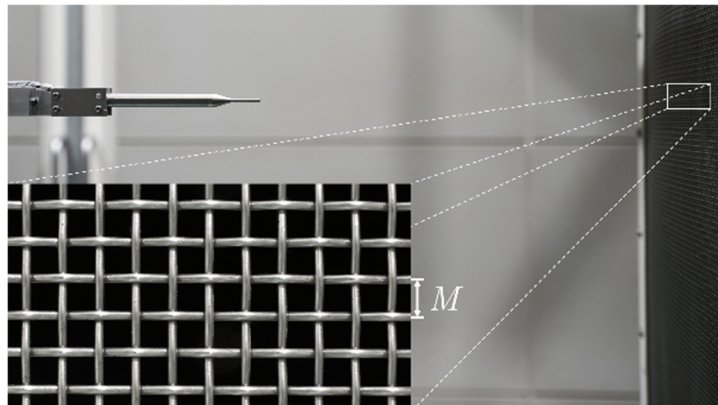


**Figure 4. Wind tunnel setup with the FRAP being installed downstream of the grid in the nozzle section**

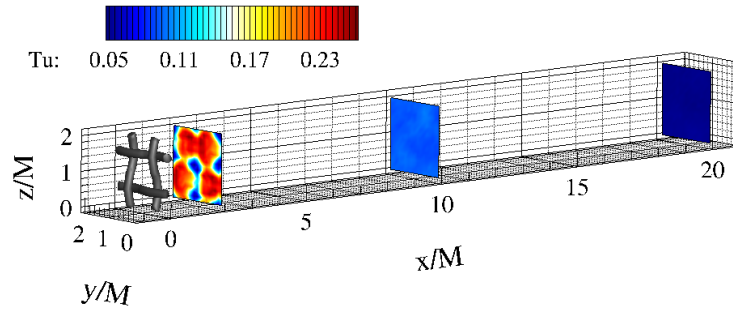


**Figure 5. Homogeneity of the flow downstream of the grid at  $x/M = \{2, 10, 20\}$  indicated by the turbulence intensity  $Tu$**

## RESULTS AND DISCUSSION

In a first evaluation step, the assumptions made regarding homogeneous isotropic turbulence are evaluated as a prerequisite for the application of Taylor's frozen turbulence hypothesis.

The first assumption is the homogeneity of the flow field. Hence, three measurement planes with a very fine measurement grid resolution ( $\Delta y = \Delta z = M/8 = 0.8 \text{ mm}$ ) are measured in the near wake of the grid at  $x/M = \{2, 10, 20\}$ . Contour plots of the turbulence intensity  $Tu$  at the measurement planes at  $Re_M = 4300$  are shown in Figure 5. In the near-field of the grid, the flow field is very inhomogeneous due to the separation and acceleration of the flow at the grid. At  $x/M = 10$  the flow field is still strongly influenced by the grid, resulting in a very homogeneous flow field at  $x/M = 20$ .

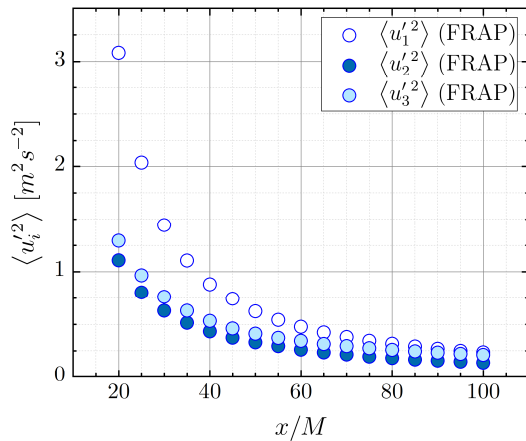


**Figure 6. Velocity components variance downstream of the grid as a characteristics for isotropy**

In order to investigate the assumption of isotropy, the degree of anisotropy is observed with the FRAP downstream of the grid. In Figure 6, the variances of the three velocity fluctuation components are depicted. As described in the literature, the component in streamwise direction is higher compared to the lateral and vertical components. The difference is decreasing with a larger distance

from the grid. From  $x/M \geq 40$  the flow gets more and more isotropic. Hence, the assumption of isotropy holds for measurements in the far wake of the grid.

The investigation of higher order statistical moments of the velocity magnitude, like the non-dimensional third order moment in Figure 7 for both Reynolds numbers, shows that the assumption of homogeneity holds at distances  $x/M \geq 40$ . The third order statistical moment is very low and almost constant for farther downstream measurement points.

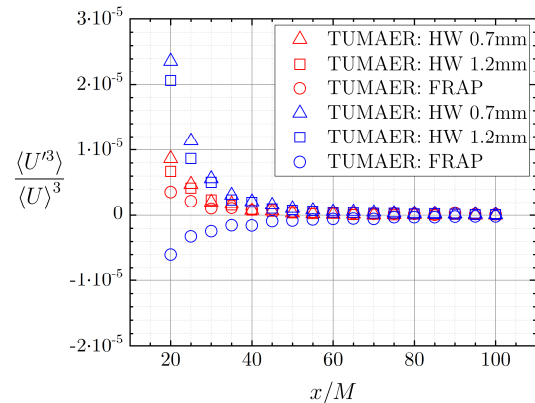


**Figure 7. Normalized third order statistical moment for  $Re_M = 4300$  (red) and  $Re_M = 12800$  (blue)**

Figure 8 shows the local, normalized velocity variance for all probes under investigation and validation data from the literature (Ashok et al. (2012)). The trend that the smaller the spatial filtering due to the probe size, the higher the measured variance, can be observed in both, the literature and the measurement data at TUM-AER. Interestingly, the five-hole probe with a head diameter of  $3 \text{ mm}$  lies between the two single-wire probes used for validation purposes. The reason why the TUM-AER single-wire probe with a wire length of  $0.7 \text{ mm}$  lies below the  $1 \text{ mm}$  probe in the literature is due to the lack of comparability in the length to diameter ratio of the various probes. Ashok et al. used wires with smaller diameters to compensate for 3D flow effects around the hot-wire.

The ratio of the wire length to the wire diameter  $l_w/d_w$  is larger by a factor of at least 2 for all measurements of Ashok et al. An additional reason for the deviation of the measurements from the literature to the measurements at TUM-AER is related to the differences in the flow in the wind tunnel, i.e. wind tunnel effects.

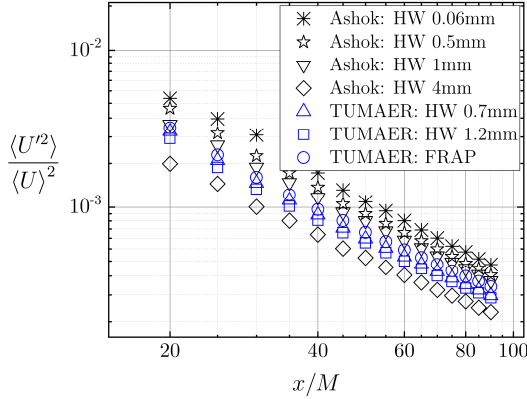


**Figure 8. Local normalized velocity variance at  $Re_M = 12800$**

As described in eqn. (4), the dissipation rate of the flow can be deduced from the spatial derivative of the velocity components variances, when assuming homogenous, isotropic turbulence and Taylor's frozen turbulence hypothesis. In Figure 9, the dissipation rate for both Reynolds number cases is displayed for a) the dissipation rate calculated with the present 3D variances, viz. without the homogenous isotropic turbulence (HIT), and b) with the HIT approximation. Due to the described higher degree of anisotropy in the near wake, the approximation overestimates the dissipation rate throughout the full traverse in downstream direction, but still follows the estimated trend.

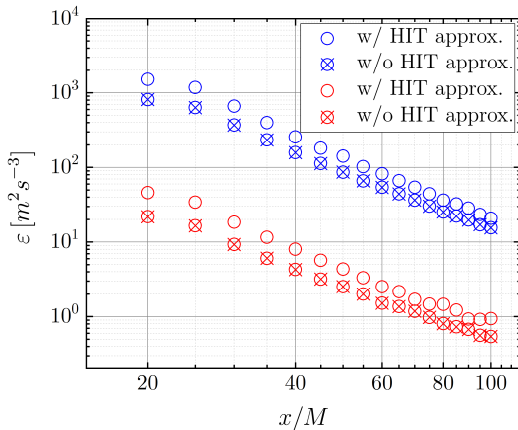


**Figure 9. FRAP Dissipation rate for  $Re_M = 4300$  (red) and  $Re_M = 12800$  (blue) with and without the homogeneous isotropic turbulence (HIT) approximation in eqn. (4)**

In the literature, values for the Reynolds number based on the Taylor micro scale lie in the range  $Re_\lambda = (30, 80)$  (see Ashok et al. (2012)). The measurements from the FRAP  $Re_\lambda = (42, 68)$  match the reference data. Furthermore, the Kolmogorov length scale  $\eta$ , calculated as defined in eqn. (7), is shown in Figure 10 for both Reynolds numbers. For  $Re_M = 12800$ , the data for both measurement techniques match very well in the entire  $x/M$  range downstream of the grid. For the lower Reynolds number, deviations between the hot-wire measurements and the FRAP occur in the far wake at distances  $x/M > 80$ . This is mainly due to the low velocity fluctuation magnitudes. Small velocity fluctuations around a low mean velocity correspond to even smaller pressure changes, and therefore can not be resolved appropriately. It can be seen that the Kolmogorov length scale increases with increasing distance from the grid. Furthermore, it increases with decreasing Reynolds numbers. The same trend is shown in the literature with Kolmogorov length scales of  $\eta = (0.04, 0.275) \text{ mm}$  for the equivalent  $Re_M$  (see Ashok et al. (2012)).

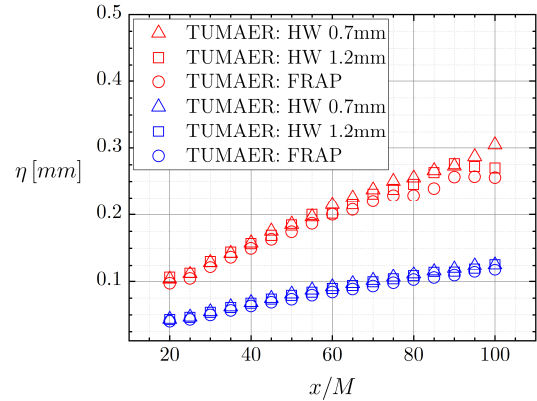


**Figure 10. Kolmogorov length scale for  $Re_M = 4300$  (red) and  $Re_M = 12800$  (blue) for the FRAP and both single wire probes**

In the spectral analyses, the acquired signals are post-processed (averaging and filtering) as described in Figure 2. In Figure 11, normalized kinetic energy spectra  $E_{kin}/(\epsilon \nu^5)^{1/4}$  for the FRAP at various downstream positions as a function of  $k\eta$  at  $Re_M = 12800$  are depicted. As a reference, the energy spectrum for the single-wire measurement at  $x/M = 50$  is given, as well. After the near constant trend in the low bandwidth region, the inertial subrange showing the  $k^{-5/3}$  dependency is reproduced by both methods. Due to the minimal resolution of the sensor-DAQ-system, the FRAP signals have been additionally low-pass filtered. Therefore, the inertial subrange can not be fully resolved by the FRAP. Since the abscissa is non-dimensionalized with the Kolmogorov length scale, which increases with the distance from the grid, the cut-off value  $k\eta$  for the FRAP measurements is

shifted for measurements farther downstream. In comparison, the single-wire measurement with a wire length of  $l_w = 1.2 \text{ mm}$  additionally resolves even smaller scales in the dissipative range of the energy cascade.

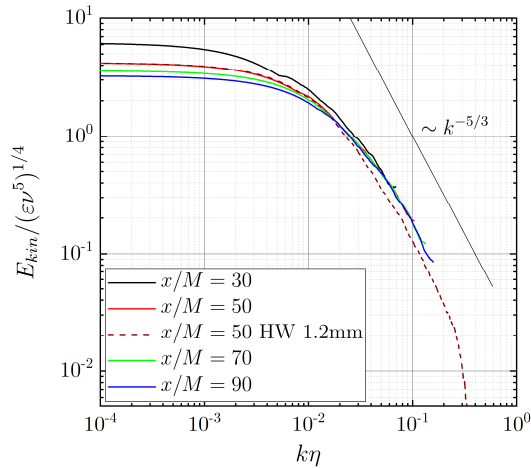


**Figure 11. Normalized kinetic energy spectra at various downstream positions as a function of  $k\eta$  for  $Re_M = 12800$**

In Figure 12, the pre-multiplied energy spectra  $kE_{kin}/(\epsilon v^5)^{1/4}$  are shown for all measured distances downstream the grid. It can be seen that the energy decreases with the distance from the grid. For all measurements, the FRAP cannot fully resolve the decay in the high bandwidth region  $k\eta > 10^{-1}$ .

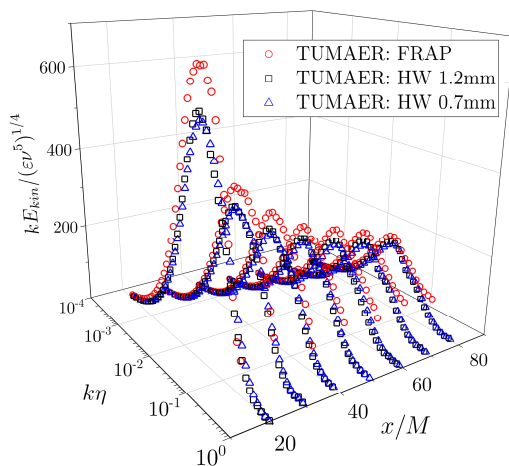


**Figure 12. Pre-multiplied normalized kinetic energy spectra as a function of  $k\eta$  for  $Re_M = 4300$**

## CONCLUDING REMARKS

In this study, grid-generated turbulence has been investigated experimentally in a low-speed wind tunnel. Data from a fast-response multi-hole pressure probe is compared to data from single-wire CTA probes and data from the literature. The underlying assumptions of homogeneity and isotropy have been studied thoroughly. The

evaluation of higher order statistics show a good agreement between the different measurement methods. Solely, minor deviations in regions with small velocity fluctuations around a low wind speed can be observed in the FRAP data. In the spectral investigations, the limits of the FRAP have been shown. These are mainly due to the minimal resolution of the FRAP sensors/DAQ system and the bandwidth limit of the experimentally acquired temporal calibration. Future developments concerning those issues should overcome the problems: Smaller probe dimensions could further reduce spatial and temporal filtering. Moreover, the limits of the piezo-resistive sensor should be avoided by the application of newly developed fiber-optic pressure sensors in the future.

## REFERENCES

- Ashok, A., Bailey, S. C. C., Hultmark, M., and Smits, A. J., 2012. Hot-wire spatial resolution effects in measurements of grid-generated turbulence. *Experiments in Fluids*, 53, p.1713-1722.
- Bailey, S. C. C., Kunkel, G. J., Hultmark, M., Vallikivi, M., Hill, J. P., Meyer, K. A., Tsay, C., Arnold, C. B., and Smits, A. J., 2010. Turbulence measurements using a nanoscale thermal anemometry probe. *Journal of Fluid Mechanics*, 663, p. 160-179.
- Bearman, P.W., 1971. Corrections for the effect of ambient temperature drift on hot-wire measurements in incompressible flow. *DISA Inf.* 11(11), p. 201-208.
- Heckmeier, F. M., Iglesias, D., Kreft, S., Kienitz, S., and Breitsamter, C., 2019. Development of unsteady multi-hole pressure probes based on fiber-optic pressure sensors. *Engineering Research Express*, 1(2), p. 025023.
- Heckmeier, F. M., and Breitsamter, C., 2020. Aerodynamic Probe Calibration using Gaussian Process Regression. *Measurement Science and Technology*.
- Kupferschmied, P., Köppel, P., Gizzi, W., Roduner, C., and Gyarmathy, G., 2000. Time-resolved measurements with fast-response aerodynamic probes in turbomachines. *Measurement Science and Technology*, 11, p.1036-1054.
- Johansen, E. S., 2001. Development of a fast-response multi-hole probe for unsteady and turbulent flowfields. Dissertation, Texas A&M University, College Station, Texas, USA.
- Pope, S., 2000. *Turbulent Flows*. Cambridge: Cambridge University Press
- Ting, D., 2016. *Basics of Engineering Turbulence*. Academic Press.